

# Is Perfect Filtering Enough Leading to Perfect Phase Correction for dMRI data?

Feihong Liu<sup>1,2</sup>, Junwei Yang<sup>3,2</sup>, Xiaowei He<sup>1,4</sup>, Luping Zhou<sup>5</sup> ✉,  
Jun Feng<sup>1,4</sup> ✉, and Dinggang Shen<sup>2,6</sup> ✉

<sup>1</sup> School of Information Science and Technology, Northwest University, Xi'an, China

<sup>2</sup> School of Biomedical Engineering, ShanghaiTech University, Shanghai, China

<sup>3</sup> Department of Computer Science and Technology, University of Cambridge, Cambridge, United Kingdom

<sup>4</sup> State-Province Joint Engineering and Research Center of Advanced Networking and Intelligent Information Services, School of Information Science and Technology, Northwest University, Xi'an, China

<sup>5</sup> School of Electrical and Information Engineering, University of Sydney, Sydney, Australia

<sup>6</sup> Shanghai United Imaging Intelligence Co., Ltd., Shanghai, China  
luping.zhou@sydney.edu.au, fengjun@nwu.edu.cn, dgshen@shanghaitech.edu.cn

**Abstract.** Being complex-valued and low in signal-to-noise ratios, magnitude based diffusion MRI is confounded by the noise-floor that falsely elevates signal magnitude and incurs bias to the commonly used diffusion indices, such as fractional anisotropy (FA). To avoid noise-floor, most existing phase correction methods explore improving filters to estimate the noise-free background phase. In this work, after diving into the phase correction procedures, we argue that even a perfect filter is insufficient for phase correction because the correction procedures are incapable of distinguishing sign-symbols of noise, resulting in artifacts (*i.e.*, arbitrary signal loss). With this insight, we generalize the definition of noise-floor to a complex polar coordinate system and propose a calibration procedure that could conveniently distinguish noise sign-symbols. The calibration procedure is conceptually simple and easy to implement without relying on any external technique, while keeping distinctly effective. Extensive experimental results, including those on both synthetic and real diffusion MRI data, demonstrate that the calibrated procedures successfully mitigate artifacts in diffusion MR images and FA maps, with improved accuracy on estimating FA in particular.

## 1 Introduction

Diffusion-weighted (DW) imaging enables reliably characterizing white-matter microstructure in-vivo. Using large  $b$ -values for more diffusion weighting during imaging, DW signals on one hand could be acquired in high resolution [1], but on the other hand are inherently susceptible to low signal-to-noise ratio (SNR) [2]. As DW signal is by nature complex-valued, low SNR magnitude based image

regions, especially for those in absence of signal, are superimposed by the well-known noise-floor which falsely elevates signal magnitude, incurring estimation bias to the commonly used diffusion indices, *e.g.*, fractional anisotropy (FA) [3].

To avoid the noise-floor, instead of reconstructing magnitude, a preprocessing technique named phase correction is employed, which complex-rotates the DW signal so that its real part carries the true signals plus Gaussian distributed noise and its imaginary part contains purely noise that will be discarded. The complex rotation is guided by the background phase, estimated by smoothing real and imaginary signals, respectively. An early phase correction approach employs total variation (TV) [3] for signal smoothing, achieving reliable performance in white-matter characterization. That work also pointed out the direction in catering TV for spatially-varying noise caused by the multi-coil parallel imaging approach.

The advance of current phase correction technique is reflected by exploring filters accounting for the noise variability. To improve TV, a great deal of analyses have been implemented to evaluate the function of its regularization parameter (*i.e.*,  $\lambda$ ) [4]. Those works pave to proposing weighted TV (wTV) that generates voxel-wise weights to adjust  $\lambda$  according to the estimation of noise-level [5]. As anticipated, wTV effectively eliminates artifacts, however, the evaluation of its filtering performance was left in those works. After that, multi-kernel filtering was put forward, which is based on bilateral filtering and adapts the range kernel parameter voxel-wisely to spatially-varying noise and mitigates the artifacts with a better filtering performance [6]. Following that, an improved filtering approach for noise-level estimation was also proposed [7], however, the cross-sectional comparison of its filtering capacity was still not provided.

Meanwhile, two interesting phenomena have attracted our attention. First, wTV that performs well in removing artifacts in DW images and FA maps achieves inferior performance on the intermediate filtering results, possibly due to the compromise between regularization adaptivity and filtering capacity. Second, in contrast to wTV, Marchenko–Pastur principal component analysis (MP-PCA) [8], which allows accurate estimation of noise-level, surprisingly introduces considerable artifacts in the DW images and FA maps. Both phenomena suggest that patching filters might just be a half-measure and that there could be some underlying problems behind phase correction procedures, hindering the noise-floor suppression.

To further investigate this problem, in this paper, we employ the complex polar coordinate system, which is a combination of polar coordinate and Cartesian coordinate, to cautiously analyze the procedures of phase correction and to insightfully generalize the definition of noise-floor. What follows, we introduce a simple but effective calibrate procedure to remedy for conventional phase correction procedures. The calibration procedure allows phase correction to conveniently distinguish noise sign-symbols, eliminating the confusion between the noise-floor and normal signals. Extensive experimental results, including those on both synthetic and real diffusion MRI data, demonstrate that calibrated procedures effectively help mitigate artifacts in phase-corrected DW images and FA maps, with improved accuracy on estimating FA in particular.

## 2 Calibration of Phase Correction Procedures

Diffusion MRI is inherently complex valued and low in SNRs. It could be corrupted by noise presented in both complex axes with changed signal sign-symbols. When reconstructing magnitude, the sum of square (SoS) operation simply flips all signal to positive. Thereby, negative contribution of magnitude turns to positive, which elevates magnitude and cannot be eliminated through averaging. While noise-floor emerges under the case that SoS neglects noise sign-symbols, significant signal loss appears under the case that phase correction neglects the sign-symbols. This issue has not been sufficiently studied for the long term seemingly because the negative contribution to magnitude cannot be analyzed in the commonly used polar coordinate. In this section, with a goal to unveil how phase correction inherently introduces artifacts to images, we utilize the complex polar coordinate system to comb through phase correction procedures and noise-floor (Section 2.1), and accompanied with a generalized definition of noise-floor, we put forward a rule of thumbnail for discerning noise-floor accurately (Section 2.2).

### 2.1 Indiscernibility of Noise Sign-Symbols Results in Signal Loss

The complex-rotation employed by phase correction can be formulated in a polar coordinate:

$$I^{\text{PC}}(\mathbf{x}) = M(\mathbf{x})e^{j\Delta\varphi(\mathbf{x})}, \quad (1)$$

where  $\mathbf{x}$  denotes a voxel location and  $\Delta\varphi(\mathbf{x}) = \varphi(\mathbf{x}) - \varphi_{\text{BG}}(\mathbf{x})$  is the rotation angle. Given the noisy magnitude  $M(\mathbf{x})$  and the phase  $\varphi(\mathbf{x})$ , the phase-corrected result  $I^{\text{PC}}(\mathbf{x})$  is determined by the background phase  $\varphi_{\text{BG}}(\mathbf{x})$ ,

$$\varphi_{\text{BG}}(\mathbf{x}) = \arctan \frac{f(I_i(\mathbf{x}))}{f(I_r(\mathbf{x}))}, \quad (2)$$

where  $f(\cdot)$  denotes a filtering operator on the real part  $I_r(\mathbf{x})$  and the imaginary part  $I_i(\mathbf{x})$  of DW signal, respectively.

At the same time, the complex-rotation can also be formulated in a Cartesian coordinate. In this case, the phase-corrected image  $I^{\text{PC}}(\mathbf{x})$  can be written as

$$I^{\text{PC}}(\mathbf{x}) = I_r^{\text{PC}}(\mathbf{x}) + jI_i^{\text{PC}}(\mathbf{x}). \quad (3)$$

Combining Eqn. 1 and Eqn. 3, the phase-corrected real part  $I_r^{\text{PC}}(\mathbf{x})$  and imaginary part  $I_i^{\text{PC}}(\mathbf{x})$  are given by

$$\begin{cases} I_r^{\text{PC}}(\mathbf{x}) = M(\mathbf{x}) \cos(\Delta\varphi(\mathbf{x})), \\ I_i^{\text{PC}}(\mathbf{x}) = M(\mathbf{x}) \sin(\Delta\varphi(\mathbf{x})). \end{cases} \quad (4)$$

Please note that, by the complex-rotation, the imaginary part  $I_i^{\text{PC}}(\mathbf{x})$  purely contains noise and will be discarded in phase correction, while the real part  $I_r^{\text{PC}}(\mathbf{x})$  is used as the corrected magnitude corresponding to  $M(x)$ .

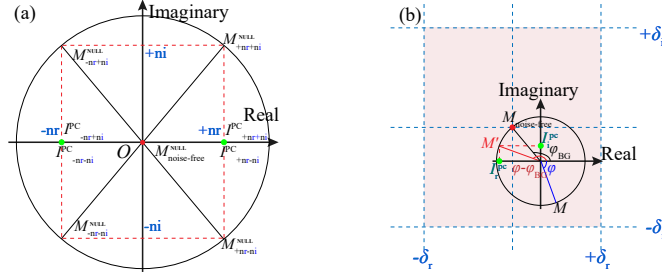


Fig. 1: (a) The complex polar coordinate system, with a noise-free complex voxel that is in absence of signal at the origin (*i.e.*,  $M_{\text{noise-free}}^{\text{NULL}} = 0$ ), enables to analyze the negative contribution to magnitude. The negative contribution is derived from noise-floor, denoted by  $I_{-nr,-ni}^{\text{PC}}$ . (b) The noise-floor deflects noise-free voxel  $M_{\text{noise-free}}$  to  $M$  that locates at the diagonal quadrant of the opposite side.  $\delta_r$  and  $\delta_i$  denote that the noise level in imaginary and real parts are the same.

To unveil how phase correction inherently introduces artifacts to images, we borrow the complex polar coordinate system, which is a mixture of the Cartesian and the Polar coordinate systems, and study noise-floor in a simplified scenario as shown in Fig. 1(a). We specifically exploit a noise-free complex voxel that is in absence of signal, with the magnitude  $M_{\text{noise-free}}^{\text{NULL}} = 0$ , marked by the red dot at the origin, *i.e.*,  $Z = 0 + j0$ . Let us suppose  $M_{\text{noise-free}}^{\text{NULL}}$  is corrupted by four cases of complex noises, all of which have the same values for the real and the imaginary components (*i.e.*,  $nr = ni > 0$ ) but with different sign-symbols (*i.e.*,  $\pm nr$  and  $\pm ni$ ). Accordingly, this leads to four corrupted voxels with their magnitudes (denoted as  $M_{-nr,-ni}$ ,  $M_{-nr,+ni}$ ,  $M_{+nr,-ni}$ , and  $M_{+nr,+ni}$  and located at different quadrants in the complex polar coordinate system). And their corresponding phase corrected magnitudes are denoted as  $I_{-nr,-ni}^{\text{PC}}$ ,  $I_{-nr,+ni}^{\text{PC}}$ ,  $I_{+nr,-ni}^{\text{PC}}$ , and  $I_{+nr,+ni}^{\text{PC}}$ , respectively, with their relationships shown in Fig. 1(a).

Let us consider only  $M_{-nr,-ni}$  (in the third quadrant) and  $M_{+nr,+ni}$  (in the first quadrant) first. When reconstructing  $M_{-nr,-ni}$ , the noises are typically flipped from negative to positive, resulting in noise-floor that elevates magnitude in a postprocessing average step, due to  $M_{-nr,-ni} + M_{+nr,+ni} > 0$ . For this case, the phase correction could avoid the noise-floor since  $I_{-nr,-ni}^{\text{PC}} + I_{+nr,+ni}^{\text{PC}} = 0$ , assuming  $\varphi_{\text{noise-free}}^{\text{NULL}} = 0$ .

However, Fig. 1(a) also demonstrates an inherent issue of phase correction procedures. When considering  $M_{-nr,-ni}$  (in the third quadrant) and  $M_{-nr,+ni}$  (in the second quadrant), their phase corrected results become  $I_{-nr,+ni}^{\text{PC}} = I_{-nr,-ni}^{\text{PC}}$ , which is quite counter-intuitive, because in the context of noise-floor  $I_{-nr,+ni}^{\text{PC}}$  is falsely as small as  $I_{-nr,-ni}^{\text{PC}}$  after the correction. This may cause arbitrary signal loss and thus artifacts (such as black holes) in DW images and FA maps.

## 2.2 Noise-Floor Restatement and Phase Correction Calibration

Inspired by the above observation, in this section, we first give a lemma to generalize the scenarios causing noise-floor, then propose a theorem to unveil how to discern the noise-floor from normal signals, and ultimately develop a calibration remedy for the conventional phase correction. *Given a perfect filter*, we can find that noise-floor occurs when the following condition is met.

**Lemma 1.** *The noise-floor is caused by noises with different sign-symbols to the low-SNR complex signals, typically appearing when the complex noises deflect the noise-free signal to the diagonal quadrant on the opposite side in the complex polar coordinate system.*

Lemma 1 can be pictorially illustrated by Fig. 1(b). Compared with the magnitude  $M_{\text{noise-free}}^{\text{NULL}}$  that is in absence of signal in Fig. 1(a), the real and imaginary signals of a low-SNR voxel  $M_{\text{noise-free}}$  may have either positive or negative sign-symbols. Thus, the concept of ‘negative’ contribution to magnitude should be generalized accordingly. From the given case in Fig. 1(b) (more cases are in our supplementary materials), the sign-symbols of both signals are changed when super-imposed with noises. Thus, the sum of square approach falsely accumulates the noise rather than the true signal because the inverted signal with different sign-symbol is purely noise. Even dramatically, this pure noise cannot be simply suppressed by averaging in postprocessing procedures, because its distribution has been changed to Rician or non-central  $\chi$ .

**Theorem 1.** *The noise-floor, which causes the noise-free signal  $M_{\text{noise-free}}$  to deflect to the opposite diagonal quadrant, always has a complex-rotation angle that is between  $\pi/2$  and  $3\pi/2$ , and the resulting noise-floor-superimposed magnitude  $M'$  always locates at the second or the third quadrant, and vice versa.*

*Proof. Sufficiency:* Because when rotating a complex signal to the opposite diagonal quadrant, the rotation should pass a full quadrant; we have  $\Delta\varphi(\mathbf{x}) > \pi/2$ , while  $\Delta\varphi(\mathbf{x}) < 3\pi/2$  is obvious. In addition, since the  $\Delta\varphi(\mathbf{x})$  is the phase of the complex-rotated magnitude  $M'$ , leading to  $M'$  always locating at the second or the third quadrant within the range  $[\pi/2, 3\pi/2]$ . *Necessity:* Given a noisy signal  $M$  at the opposite diagonal quadrant of  $M_{\text{noise-free}}$ , assume it is not noise-floor. This relationship reveals that the sign-symbols of complex signal of  $M_{\text{noise-free}}$  are totally changed. Then according to Lemma 1,  $M$  is superimposed by noise-floor, which contradicts with the assumption. The proof completes.

Guided by Theorem 1, we propose a calibration procedure for phase correction as follows:

$$I^{\text{PC}}(\mathbf{x}) = M(\mathbf{x})e^{j\Psi(\Delta\varphi(\mathbf{x}))}. \quad (5)$$

$\Psi(\cdot)$  denotes the operator to check whether  $M$  is deviated by the complex noises to the opposite diagonal quadrant of  $M_{\text{noise-free}}$ . The calibration procedure is summarized in Algorithm 1.

---

**Algorithm 1** Phase calibration for discerning noise-floor

---

**Input:**  $\varphi(\mathbf{x})$  and  $\varphi_{\text{BG}}(\mathbf{x})$  estimated by Eqn. 2**Output:**  $\Delta\varphi(\mathbf{x})$  to be used in Eqn. 4 for phase correction

- 1: **repeat**
  - 2:   set  $\Delta\varphi(\mathbf{x}) = \varphi(\mathbf{x}) - \varphi_{\text{BG}}(\mathbf{x})$ ;
  - 3:   if  $\Delta\varphi(\mathbf{x})$  is in the 2-nd or 3-rd quadrant, then flip it to the 1-st or 4-th quadrant, respectively, marked by  $\Delta\varphi^{\text{f}}(\mathbf{x})$ ;
  - 4:   if  $\Delta\varphi(\mathbf{x})$  deflects  $M_{\text{noise-free}}$ , estimated from filtering real and imaginary signals, to  $M$  that locates at the opposite diagonal quadrant, then flip  $\Delta\varphi^{\text{f}}(\mathbf{x})$  back to the 2-nd or 3-rd quadrant, marked by  $\Delta\varphi^{\text{ff}}(\mathbf{x})$ ;
  - 5:   if  $\Delta\varphi(\mathbf{x}) \neq \Delta\varphi^{\text{ff}}(\mathbf{x})$ , then replace  $\Delta\varphi(\mathbf{x})$  by  $\Delta\varphi^{\text{f}}(\mathbf{x})$ ;
  - 6: **until** all voxels have been processed.
- 

### 3 Experimental Results

#### 3.1 Datasets

We employed both synthetic and real data to demonstrate the effectiveness of the calibrated procedures for phase correction. We synthesized the background phase according to [4], and generated synthetic DW data using Phantom $\alpha$ s [9], with the same gradient vectors of the real DW data described as follows. With the noise-free DW data, we added spatially-varying Gaussian noises to the real and imaginary parts, respectively [10]. The real DW data were acquired using a SIEMENS 3T Magnetom Prisma MR scanner with following protocol, TR = 2500 ms, TE = 89 ms, FoV =  $210 \times 210 \text{ mm}^2$ , matrix size =  $140 \times 140$ , and  $b = 750, 1500, 3000 \text{ s/mm}^2$  with a total of 64 diffusion directions.

#### 3.2 Experimental Settings

We chose the optimal filtering parameters based on the synthetic data and applying them to processing the real DW signal. To verify the effectiveness of our proposed calibration method, we compared phase correction performance before and after the calibration. The parameters used in the phase correction are set as follows. For TV denoising (denoted as TV), the regularization parameter  $\lambda$  was set as 2, and the iteration limit was set as 10. For Curvature Filtering (denoted as CF), the iteration limit used by Gaussian curvature filter was set as 10. For MPPCA denoising (denoted as MPPCA), the block size was set as  $5 \times 5 \times 5$ .

#### 3.3 Evaluation Criteria

The calibrated phase correction is expected to mitigate artifacts in DW images and FA maps. To verify this, on the synthetic data, since the ground-truth is known, we could quantitatively calculate the mean absolute error (MAE, *i.e.*, the voxel-wise absolute error averaged across a volume) between the generated and the ground-truth DW images and the mean error (ME, *i.e.*, average voxel-wise

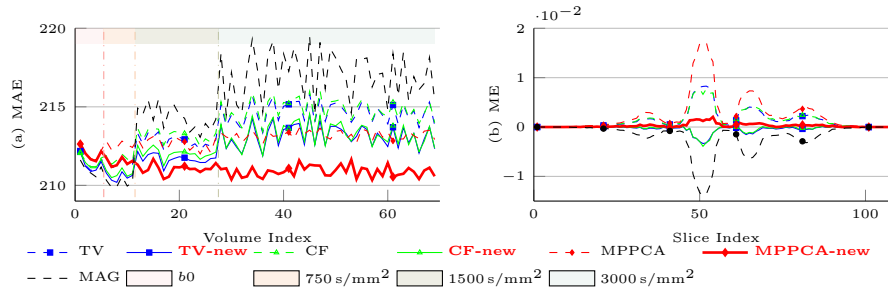


Fig. 2: Quantitative comparison on the synthetic data. (a) MAE on each DW image (volume), and (b) ME of each slice on FA maps.

error) within the white-matter regions between the generated and the ground-truth FA maps. On the real data, since the ground-truth is unavailable, we could only qualitatively evaluate the performance based on the criterion that a good phase correction is expected to lead to enhanced contrast in DW images and increased FA values in the white-matter regions, without introducing artefacts.

### 3.4 Results And Discussions

We compared (i) the phase correction performance before and after calibration, and (ii) the performance of three different filters under the same experimental setting, including CF [11], TV [12], and MPPCA [8]. Their counterparts using the proposed calibration procedure are denoted as “CF-new”, “TV-new”, and “MPPCA-new”, respectively.

**Results on synthetic data** Fig. 2 shows the quantitative results on synthetic data. On the left shows the MAE of DW images, and on the right shows the ME of FA maps. MAG (the black dashed line) denotes the magnitude of DW signals without phase correction. As can be seen, it produces much higher MAE on DW images, as well as higher ME on FA maps, than those phase correction based methods. Meanwhile, comparing phase correction with (indicated by solid lines) and without (indicated by dashed lines) the proposed calibration procedure, it can be seen that by using calibration, the produced MAE of DW image and ME of FA maps could be significantly reduced. Among all methods, MPPCA-new (*i.e.*, MPPCA with calibration) achieves the best performance with the lowest MAE and ME values.

Fig. 3 provides a visual comparison of the phase-corrected FA maps derived from synthetic data. As can be seen, phase correction brings increased FA values in white-matter regions when compared with the magnitude MAG without correction. It is also found that conventional phase correction significantly introduces artifacts that excessively enlarge FA. This phenomenon is double confirmed by the error maps shown in the second row, where the calibrated phase corrections “FA-new”, “CF-new”, and “MPPCA-new” yield less errors as indicated

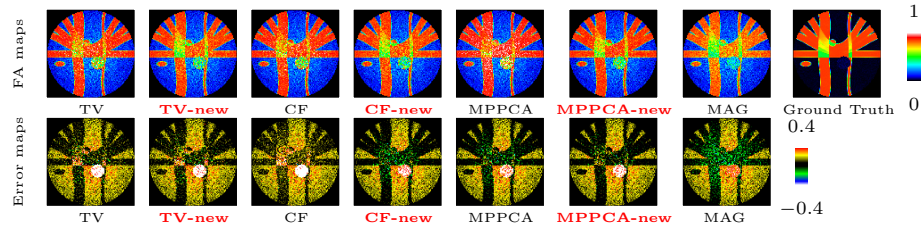


Fig. 3: Visual comparison on synthetic data. Top: FA maps; Bottom: Error maps.

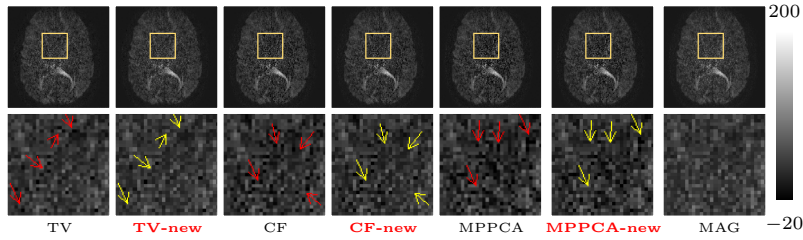


Fig. 4: Phase-corrected DW images ( $b = 3000 \text{ s/mm}^2$ ). Red/yellow arrows denote dark holes introduced/mitigated by conventional/calibrated phase correction.

by more black regions in the error maps, indicating an improved accuracy on estimating FA, especially for “MPPCA-new”.

**Results on real data** Due to lack of ground-truth, qualitative analysis was conducted to investigate the proposed calibrated phase correction on real data. Fig. 4 demonstrates phase-corrected DW images with enhanced contrast when compared to MAG that is without correction. In addition, it is found that calibrated procedures yield much fewer dark holes at image regions as indicated by the red arrows where intensities are coherently higher than surrounding regions. As reported by [13], dark holes are also reflected by artifact in FA maps shown in Fig. 5. The calibrated phase correction successfully mitigates dark holes in DW images as shown in Fig. 4 and consequently results in clean FA maps as shown in Fig. 5. Moreover, we can also find that the corpus callosum region shows enlarged FA values, which is consistent with the results documented in [3].

In sum, our results sufficiently demonstrate that conventional phase correction is also the cause of introducing artifacts. With the proposed simple calibration procedure, aforementioned artifacts could be successfully mitigated in both DW images and FA maps.

## 4 Conclusions

Recent efforts in mitigating artifacts in DW images lie in adapting filters to the spatial variability of noise. In this paper, for the first time, we propose that



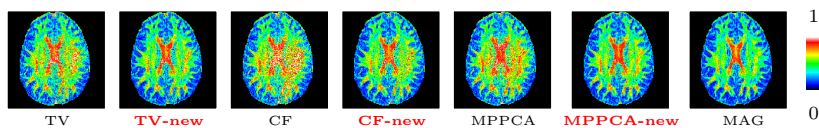


Fig. 5: FA maps obtained by phase correction without and with the calibration. Artifacts are significantly mitigated for all three filtering methods, while the FA values in corpus callosum are increased properly, after using calibration.

even a perfect filter is insufficient for phase correction. By combing through the phase correction procedures in the complex polar coordinate system, we find that they are incapable of distinguishing sign-symbols of noise and confuse the noise-floor with other normal signals. To bridge this gap, we propose a theorem and tactically develop a calibration procedure as the remedy, which is conceptually simple but distinctively effective as demonstrated by our experimental results.

## References

1. Tuch, D.S., Reese, T.G., Wiegell, M.R., Makris, N., Belliveau, J.W., Wedeen, V.J.: High angular resolution diffusion imaging reveals intravoxel white matter fiber heterogeneity. *Magnetic Resonance in Medicine* **48**(4) (2002) 577–582
2. Aja-Fernández, S., Vegas-Sánchez-Ferrero, G.: Statistical analysis of noise in MRI. Switzerland: Springer International Publishing (2016)
3. Eichner, C., Cauley, S.F., Cohen-Adad, J., Möller, H.E., Turner, R., Setsompop, K., Wald, L.L.: Real diffusion-weighted MRI enabling true signal averaging and increased diffusion contrast. *NeuroImage* **122** (2015) 373–384
4. Pizzolato, M., Fick, R., Boutelier, T., Deriche, R.: Noise floor removal via phase correction of complex diffusion-weighted images: Influence on DTI and Q-space metrics. In: MICCAI Workshop on Computational Diffusion MRI, Springer (2016) 21–34
5. Pizzolato, M., Deriche, R.: Automatic and spatially varying phase correction for diffusion weighted images. In: 26th annual meeting of the International Society for Magnetic Resonance in Medicine (*ISMRM*). (2018)
6. Liu, F., Chen, G., Feng, J., Yap, P.T., Shen, D.: Gaussianization of diffusion MRI data using spatially adaptive phase correction. In: 27th annual meeting of the International Society for Magnetic Resonance in Medicine (*ISMRM*). (2019)
7. Pizzolato, M., Gilbert, G., Thiran, J.P., Descoteaux, M., Deriche, R.: Adaptive phase correction of diffusion-weighted images. *NeuroImage* **206** (2020) 116274
8. Veraart, J., Novikov, D.S., Christiaens, D., Ades-Aron, B., Sijbers, J., Fieremans, E.: Denoising of diffusion MRI using random matrix theory. *NeuroImage* **142** (2016) 394–406
9. Caruyer, E., Daducci, A., Descoteaux, M., Houde, J.C., Thiran, J.P., Verma, R.: Phantoms: A flexible software library to simulate diffusion MR phantoms. In: 22nd annual meeting of the International Society for Magnetic Resonance in Medicine (*ISMRM*). (2014)

10. Chen, G., Dong, B., Zhang, Y., Lin, W., Shen, D., Yap, P.T.: Denoising of diffusion MRI data via graph Framelet matching in XQ space. *IEEE Transactions on Medical Imaging* **38**(12) (2019) 2838–2848
11. Gong, Y., Sbalzarini, I.F.: Curvature filters efficiently reduce certain variational energies. *IEEE Transactions on Image Processing* **26**(4) (2017) 1786–1798
12. Rudin, L.I., Osher, S., Fatemi, E.: Nonlinear total variation based noise removal algorithms. *Physica D: Nonlinear Phenomena* **60**(1-4) (1992) 259–268
13. Liu, F., Feng, J., Chen, G., Shen, D., Yap, P.T.: Gaussianization of diffusion MRI data using spatially adaptive filtering. *Medical Image Analysis* **68** (2020) 101828